Discriminating Dolomitization of Marble in the Ludwig Skarn near Yerington, Nevada Using High-Resolution Airborne Infrared Imagery*

Donald S. Windeler, Jr. and *Ronald J. P. Lyon*
Department of Applied Earth Sciences, Stanford University, Stanford, CA 94305-2225

ABSTRACT: Geoscan Mk II airborne visible and infrared imagery at 6-m resolution was compared to geologic mapping to investigate its utility in the delineation of hydrothermal dolomitization of a limestone unit in the Singatse Range near Yerington, Nevada. The imagery was processed by contrast stretching of difference images and corrected to "apparent reflectance" using laboratory spectra to obtain offset corrections. Alteration maps at scales of 1:2400 by Harris (1979) and 1:600 by the first author were considered. At both scales, good to very good correlations were achieved between the processed imagery and geologic mapping. The ready discrimination between two carbonate lithologies is a result of marked differences in the reflectance spectra of the host marble and the hydrothermal dolomite. Petrographic textures, particle sizes, and the presence of impurities are considered as possible sources of this spectral variation.

INTRODUCTION

RATIONALE FOR STUDY

THE UTILITY OF REMOTE SENSING in the evaluation of hydrothermal alteration associated with ore deposits has been the topic of numerous studies, especially in the porphyry-copper systems common in the western U.S. A type of alteration commonly associated with granitic plutons but rarely subjected to remote sensing studies is the replacement of carbonate lithologies by calc-silicates such as garnet and pyroxene. The resulting skarns can host high-grade deposits of copper, gold, iron, lead, zinc, or tungsten (Einaudi *et al.*, 1981). They have often been neglected by remote sensing workers due to their small size and the lack of visible/short-wave infrared spectral features in the calc-silicates.

The Ludwig skarn in the Yerington district of western Nevada is an optimal locale to study this type of alteration using remote methods. The Ludwig skarn is well-exposed in an arid environment with little vegetation. The geology of the area has been extensively documented, dating back to Knopf in 1918; more recent workers are referenced later. This paper is the first in a continuing study of this deposit using the Geoscan Mk II airborne multispectral scanner.

INSTRUMENTATION

Airborne spectral imagery at 6 m resolution was acquired at 1436 PDT on a 7 July 1990 flight using the 24-channel Geoscan MkII scanner. The Geoscan system has ten channels in the visible-near infrared (0.522 to 0.955 μm), eight channels in the short-wave infrared (2.044 to 2.352 μm), and six channels in the thermal infrared (8.64 to 11.28 μm). This study considers only the VNIR and SWIR data; for a discussion of the thermal data the reader is referred to Lyon and Honey (1991).

Data acquisition by the Geoscan system differs from most other scanning systems in that the instrument gains and offsets are not fixed, but are adjusted for the conditions present just prior to the flight. The system is flown twice over the target area. During the first flight, an operator adjusts the gains and offsets in each channel to maximize the surface contrast into an 8-bit dynamic range (0 to 255 DN). The same area is then flown a second time with the channels held constant at the new gains and offsets.

By adjusting the offset values so that the channel means all have a DN of 127, this serves to maximize incoming illumination. The Geoscan data thus effectively has been pre-corrected for the solar radiation curve (Rubin, 1991). This eliminates the necessity of calibrations such as the flat field and log-residual (Roberts *et al.*, 1986) in order to compare image data with actual reflectance. This method does require corrections for variation in the offset and gain settings; this problem will be considered in a later section.

Laboratory reflectance data of samples collected in the field were acquired using a GER IRIS Mark IV spectroradiometer. Reflectance values are calculated as percent relative to Halon standard. Reflectance curves reported in this study have been redrawn for display purposes; every effort was made to retain the actual amount of "noise" present in the original spectra.

GEOLOGY

DISTRICT GEOLOGY

The following description of the Yerington district geology is summarized from Proffett (1977). The description of the alteration of the Mesozoic sedimentary rocks and the simplified geologic map (Figure 1) are drawn from Einaudi (1977) and Harris and Einaudi (1982).

Early Mesozoic volcanic and sedimentary rocks are exposed in the southern Singatse Range near Ludwig. The McConnell Canyon volcanics are a thick pile of Late Triassic andesite and felsite flows, breccias, and sedimentary rocks cut by quartz porphyries. These are disconformably overlain by a 530-m thick sequence of Upper Triassic carbonaceous calcareous argillite, volcaniclastic sediments, and limestone. The uppermost unit, the Limestone of Mason Valley (Trl), is conformably overlain by a sequence of Late Triassic-Early Jurassic thin-bedded limestone, bedded felsitic siltstone and tuffs, and carbonaceous and calcareous argillites. These volcaniclastics and limestones are, in turn, succeeded by a thin limestone unit, bedded gypsum, and cross-bedded sandstone.

The volcanic-sedimentary sequence was then intruded by two major Middle Jurassic plutons: the Yerington batholith to the north and the younger Shamrock batholith to the south. The Mesozoic sedimentary and volcanic rocks now form a vertically plunging overturned anticline between the two intrusions. The

*Presented at the Eighth Thematic Conference on Geologic Remote Sensing, Denver, Colorado, 29 April - 2 May 1991.

PHOTOGRAMMETRIC ENGINEERING & REMOTE SENSING,
Vol. 57, No. 9, September 1991, pp. 1171–1177.

0099-1112/91/5709–1171$03.00/0

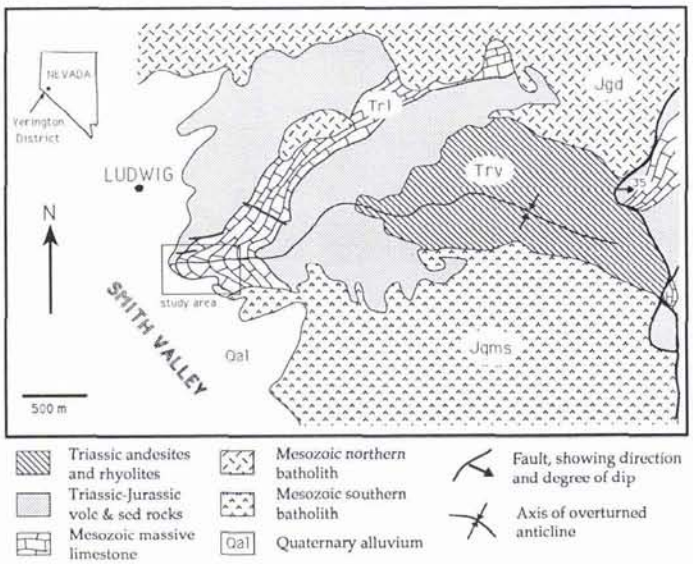

FIG. 1. Generalized geologic map of the Ludwig area, Yerington district, Nevada (after Harris and Einaudi, 1982).

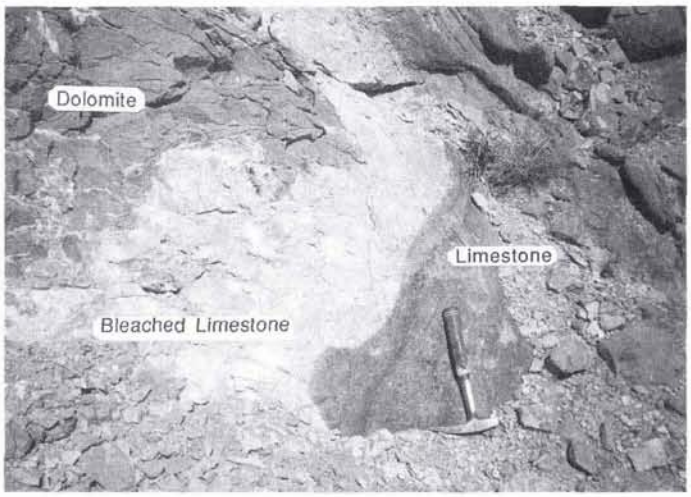

FIG. 2. Contact between limestone and dolomite.

Yerington batholith metamorphosed and hydrothermally altered much of the Mosozoic pile; the Shamrock batholith had little effect in the study area and will not be discussed further.

The first pulse of the differentiated Yerington batholith was granodioritic and caused the formation of hornfels in the limestones, silty limestones, and andesite volcanics adjacent to the intrusion. This hornfels is dominantly massive, fine-grained garnet with lesser pyroxene. Two successively smaller, more felsic pulses then followed before a swarm of quartz monozonite porphyry dikes cut both the earlier intrusions and the Mesozoic rocks. These dikes resulted in porphyry copper alteration within the batholith and skarn formation in the massive limestone unit Trl. The skarn consists of massive, coarse-grained andradite garnet formed in calcite marble and salitic diopside formed in dolomite marble.

The Mesozoic and Jurassic rocks were then rotated by later faulting. Late Mesozoic or early Tertiary faulting tilted the section 30° westward. Basin and Range faulting in the Miocene resulted in further westward tilting of 50 to 60° such that the current exposure represents a vertical cross-section through the Mesozoic rocks.

Geology of Detailed Study Area

This study examines the southernmost exposure of the Limestone of Mason Valley (Trl) on a hill with approximately 150-m vertical relief. This area offers the only good exposure of hydrothermal dolomitization of the calcite marble, an event preceding and largely overprinted by calc-silicate alteration.

Dolomitization of the marble is pervasive, leaving no relict textures. In map view, the dolomitization front cuts across bedding. At outcrop scale, however, the dolomite is clearly bedding controlled; veins of dolomite extend into the unaltered limestone parallel to dark relict bedding laminations. At the contact with the limestone, there is inevitably a zone of white, "bleached" limestone, typically 50 to 100 cm wide (Figure 2 – note that this photo represents a lateral rather than a leading edge of the dolomitization front; one of the relict bedding laminations is present to the left of the hammer). These three rock types – calcite marble, bleached limestone, and dolomite marble – are the critical lithologies in this study and are described in further detail below.

The freshest rock in the Trl unit is a blue-grey to grey calcite marble. Intrusion of the Yerington batholith resulted in recrystallization to its current coarse (2 to 5 mm) crystalline texture. Calcite is the dominant mineral phase; minor quantities of tremolite and quartz were found in thin section. Goethite pseudomorphs after pyrite and narrow veins of garnet and of talc were observed locally during field mapping, but are clearly hydrothermal. These minerals do not occur in sufficient quantities to be spectrally significant in the area of detailed study. In the balance of this study the calcite marble will usually be referred to as limestone.

The bleached limestone is a white calcite rock of variable grain size. At the contact with dolomite, the bleached limestone has a fine-grained, commonly sugary texture and may contain up to 5 percent fine-grained iron oxides. The bleached limestone in some cases extends many metres beyond the terminus of the dolomite veins; with distance from the dolomite contact the bleached limestone regains the coarsely crystalline texture of the calcite marble and loses the iron oxide grains.

The dolomite marble is an off-white rock (light orange to brown where iron-stained) that weathers to a dull buff color. It is finer-grained (0.5 to 2 mm) than the calcite marble and is much more competent. Where dolomitization is not as intense, the dolomite exhibits a greyer color but retains the fine grain size.

The dolomite marble itself appears to be monominerallic dolomite, but is commonly cut by two vein types. Near the calcite marble contact discontinuous veinlets of white calcite occur locally. These are typically 2 to 5 mm in width and contain abundant goethite pseudomorphs after pyrite. The second vein type consists of iron-stained, usually cryptocrystalline quartz. These veins are typically 0.5 to 1.0 cm thick but can reach 4 cm. The quartz veins are much more common than the calcite veinlets and are not restricted in their spatial distribution. They are especially plentiful in the northeastern corner of the detailed map area, locally reaching an abundance of 40 to 50 percent of the outcrop.

COMPARISON BETWEEN MAPPING AND IMAGERY

Harris Mapping Area

Harris (1979) mapped the alteration of the Trl limestone and the overlying Trlb silty limestone at a scale of 1:2400. Figure 3 is adapted from the southernmost region studied by that worker. Figure 4 is an image of the same area in Geoscan channel 5 (0.717 μm) simulating an airphoto; the bright material between the limestone and the dark garnet hornfels in the south is a windblown sand dune. The area outlined in the east of Figure

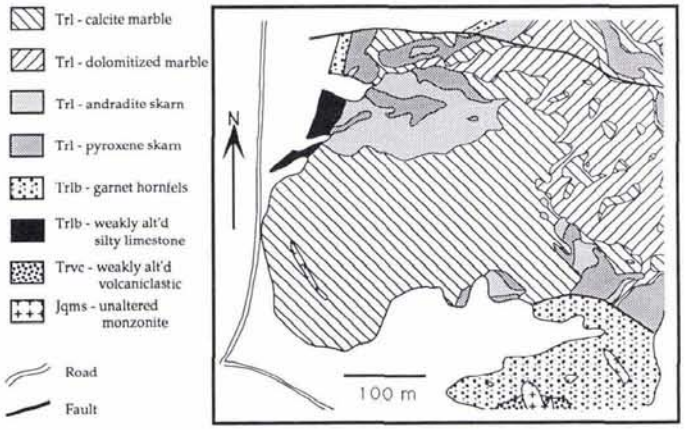

FIG. 3. Lithologic and alteration map of study area (after Harris, 1979).

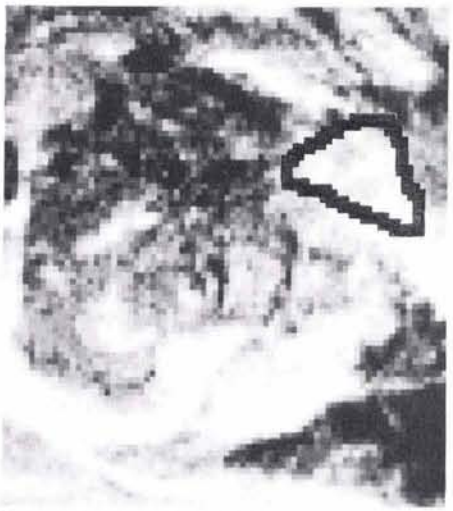

FIG. 4. Geoscan channel 5 image of Harris map area (Figure 3). The detailed study area of Figures 7 to 9 is outlined.

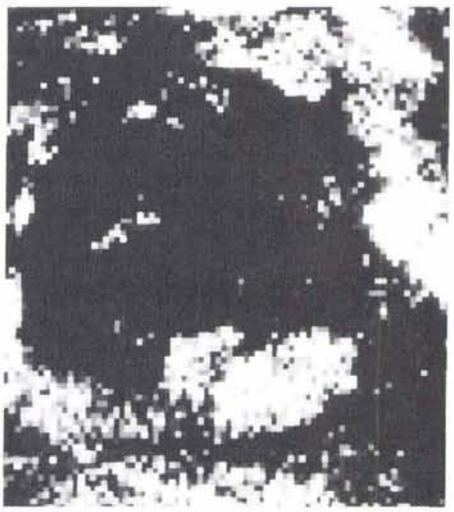

FIG. 5. Geoscan channel 7-1 image of Harris map area. Bright areas show materials with strong iron absorption.

FIG. 6. Geoscan channel 14-17 image of Harris map area. Bright areas show materials with strong carbonate absorption.

4 defines the limits of the detailed mapping described in the next section.

Figures 5 and 6 display the two image treatments that achieved the best results in discriminating between the limestone (dark) and dolomite (bright): 7-1 in the visible / near-infrared (0.830 to 0.522 μm) and 14-17 in the infrared (2.176 to 2.308 μm). Comparison between Harris' mapping of the limestone and dolomite distributions and the difference images generally show a very good correlation, although the details of the limestone "islands" within the dolomitized area have been obscured. This is probably a result of dolomite scree obscuring limestone outcrop interpreted as continuous by Harris. The 7-1 image also shows some horizontal striping (parallel to the flight direction) through the center of the limestone, which results in apparent misclassification.

One obvious discrepancy appears on the 14-17 image (Figure 6). In the western portion of the limestone, two lobate features appearing to be dolomite in the image occur in an area mapped by Harris as limestone with a small apophysis of the southern batholith. These anomalies consistently occur in the SWIR treatments of the imagery and are clearly visible in the Figure 4 "airphoto." Field checking of these anomalies prove them to be large areas of bleached limestone with minor dolomite veins. (This alteration is undoubtedly connected to the more pervasive dolomitization in the missing third dimension, as there is considerable vertical relief between the two areas.) This is the only location in the study area where the quantity of bleached limestone is sufficient to be spectrally significant; the spectral properties of this rock will be considered later.

Of these two treatments, the 14-17 difference best discriminates between dolomite and limestone. While the 7-1 treatment separates these two lithologies, it also highlights the windblown sand dunes in the southern half of the image. These sands may have a thin veneer of iron oxides; as the 7-1 treatment discriminates between the limestone and the dolomite by the higher iron content of the latter, it also defines the sand dunes. The 14-17 treatment relies on the stronger carbonate absorption feature in the dolomite and thus does not include any non-carbonate lithologies.

Detailed Mapping Area

As a means of exploring the utility of the Geoscan imagery at a very large scale, one particular area of contact between the limestone and dolomite was mapped for the present study at a scale of 1:600. Relative proportions of limestone and dolomite float were recorded as well as outcrop in order to generate a map of the true surface geology. This map was then "defocused" to Figure 7 by overlaying a 3-m grid and classifying the "pixels" as either limestone, dolomite, or mixed. The cutoffs for a "pure" pixel were arbitrarily set at 75 percent or greater of a phase. A 3-m grid was chosen so as to allow comparison with image data from another flight at 3-m resolution which proved to show some distortion; the 6-m data set showed no such distortion and thus was used for this study.

At this scale, the best image treatments were found to be 7-1 and 14-16 (Figures 8 and 9; individual pixels are 6 m). The 14-17 treatment used in Figure 6 yielded similar results but was slightly inferior to the 14-16 treatment. The correlation between the imagery and the surface map is slightly poorer than that of the imagery with the smaller scale Harris map, but still yields good results. While some loss of agreement is to be expected, there are possible explanations in addition to the simple consequences of working at such a large scale. The most likely is that the choices for cutoff values in the map classification were incorrect; 75 percent is an arbitrary value and there is no reason the cutoffs need be the same for limestone and dolomite.

An explanation for the ambivalent agreement in the northernmost dolomite could be the presence of quartz veins. While the map defocusing scheme assumed only limestone and dolomite were spectrally significant, this area has the greatest abundance of the iron-stained quartz veins and their presence could have muted the spectral features used to separate the dolomite from the limestone. This hypothesis is also supported by Figure 8, as the 7-1 treatment (emphasizing iron content) correctly identifies this northernmost area as dolomite.

SPECTRAL CHARACTERISTICS OF LITHOLOGIES

Laboratory and Geoscan Spectra

In order to understand the ready discrimination between the limestone and the dolomite in the imagery, the spectral characteristics of these materials must be considered. The visible and IR reflectance spectra of representative samples of the three rock types considered in this study were measured in bi-directional reflectance using a GER IRIS spectrometer in the laboratory. These spectra are compared in Figure 10. While both

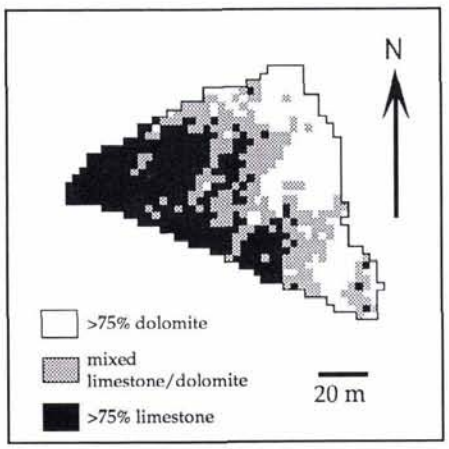

Fig. 7. Defocused surface map of detailed study area, based on field mapping. Individual pixels are 3 m.

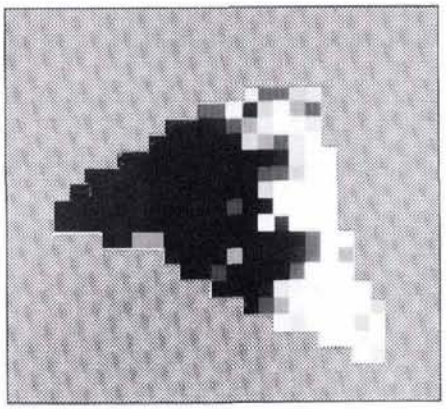

Fig. 8. Geoscan channel 7-1 image of detailed study area. Bright areas show dolomite, dark areas show limestone. Individual pixels are 6 m.

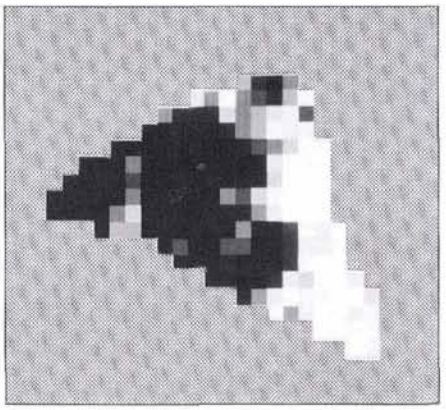

Fig. 9. Geoscan channel 14-16 image of detailed study area. Bright areas show dolomite, dark areas show limestone. Individual pixels are 6 m.

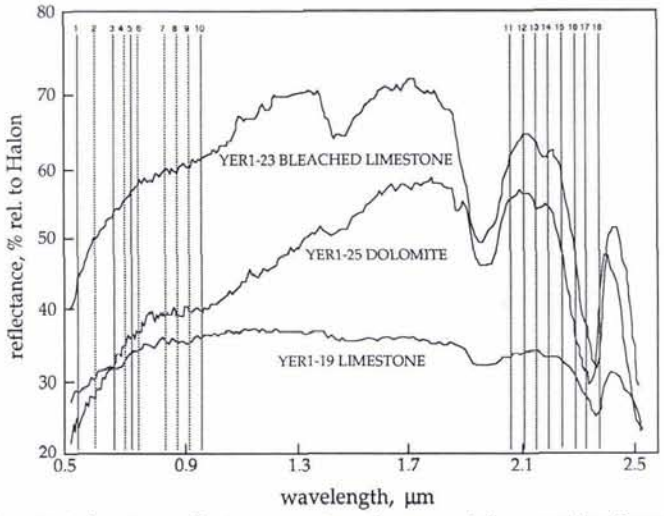

Fig. 10. Laboratory reflectance spectra of representative samples. Spectra are not offset. Geoscan band centers are included.

limestones show the CO_3^{2-} bond absorption at 2.335 μm indicative of calcite (Hunt and Salisbury, 1971), the bleached limestone otherwise appears to have more spectral similarities to the dolomite than to the spectrally flat calcite marble. As noted in the earlier discussion of the Harris map, this can result in misidentification.

The laboratory reflectance spectra presented in Figure 8 can be averaged over the same bandpasses as are present in the Geoscan system and multiplied by 2.56 to allow direct comparison with the image brightness given in an 8-bit digital number (DN). A series of plots comparing the laboratory and Geoscan data for each lithology is presented in Figure 11. The image data in these plots have been corrected using a modified version of the "dark target" or "background" corrections described by Lyon and Honey (1989).

As described earlier, offsets and gains in each channel are adjusted in flight to maximize contrast in the data before the imagery is collected. The offsets can often vary, however, as the system is calibrated for each channel while flying over unlike lithologies. The correction employed here is meant to standardize the offsets by relating the image data to the laboratory reflectance of a homogeneous, spectrally dark and featureless sample. In this study, a sample of black, carbonaceous, calcareous argillite was used as the dark sample. By subtracting the laboratory datum for each channel from its image counterpart, a set of offset correction factors is created. To avoid negative DNs in the corrected image pixels, the value of the smallest correction factor is subtracted from all 18 factors in the correction set. These correction data are then subtracted from the DN for each channel in any given pixel.

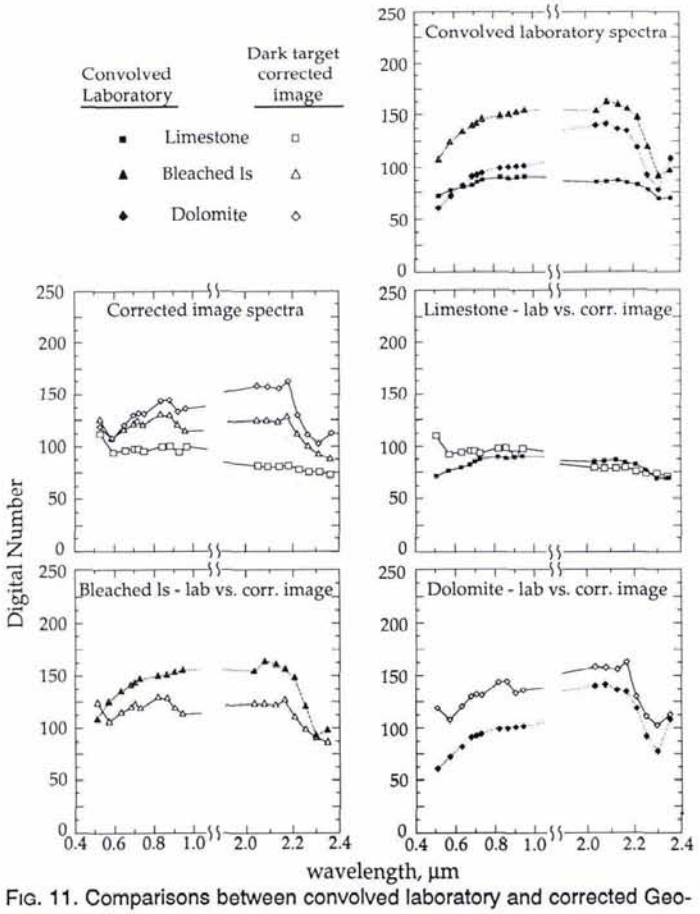

FIG. 11. Comparisons between convolved laboratory and corrected Geoscan spectra.

While this channel-by-channel correction does not account for gain settings and does not entirely remove offset errors, it is useful as a means of supplying image data with spectrally significant shapes. With the exception of the anomalously high channel 1 values, this correction results in image spectra for the limestone and dolomite that are very similar to the laboratory spectra. The bleached limestone shows a much less bright spectrum in the image data because it does not occur in large enough quantities on the imagery to extract a training set uncontaminated by the surrounding limestone. It should also be noted that this correction does not affect the results of the difference images, as the relative adjustment between two channels after correction is constant for all pixels in the image.

The corrected Geoscan spectra in Figure 11 clearly suggest which range of channel differences will be most effective in discriminating between limestone and dolomite. The buff color of the dolomite gives it a definite positive slope in the visible wavelengths as compared to the flat grey of the limestone; even with the anomalous values in channel 1, the relative differences between channels 7 and 1 can be used to discriminate between the two on the basis of color. Similarly, the well-defined 2.3-μm carbonate absorption feature in the dolomite contrasts sharply with the muted limestone spectra; this would also recommend itself as an effective discriminator in this locality.

Sources of Spectral Discrimination

This empirical approach does not, however, provide an explanation as to why these two carbonate rocks have such radically different reflectance spectra. Crowley (1986) examined variations in reflectance features of carbonates as affected by textures and impurities. He found distinct variations caused by three factors: petrographic texture, grain size, and organic impurities. The possible effects of these factors on the reflectance of the carbonates in this study will be considered individually.

Crowley defined three classes of particle textures: unskewed unimodal, skewed unimodal, and bimodal. Both the limestone and dolomite in the Trl unit are crystalline rocks with little grain size variation and would thus be classified in the first of these groups. The grain size of the bleached limestone varies, but not on the scale of a hand sample and rarely on that of an individual outcrop. As all lithologies are in the same textural class, this effect should not result in significant spectral variations.

The grain size of a carbonate rock will cause systematic variations in the reflectance characteristics. With decreasing grain size, the brightness of a sample will increase while the spectral contrast will decrease (Crowley, 1986). As the limestone has a considerably coarser grain size than the dolomite, this effect must be examined.

A sample of each rock type was crushed, sieved to various size fractions, washed to remove fine material adhering electrostatically, and dried overnight. The finest size fraction of each sample was not washed but was dried overnight with the coarser fractions. The resulting reflectance spectra for the size fractions of limestone and dolomite are presented in Figures 12 and 13, respectively. With one or two exceptions, the resulting data agree well with Crowley's observations. Reflectance shows a steady rise with decreasing grain size while contrast decreases. The variations in the spectral contrast tend to be quite subtle, however, especially in comparison with Crowley's data. The key point is that the shapes of the mineral spectra change very little; Figures 12 and 13 clearly show that particle size variations are not the cause of the dramatic contrast difference between the limestone and dolomite shown in Figure 10.

Small quantities of organic impurities in carbonates have been shown to significantly quench their spectral features. In addition, heating has been shown to increase the opacity of organic

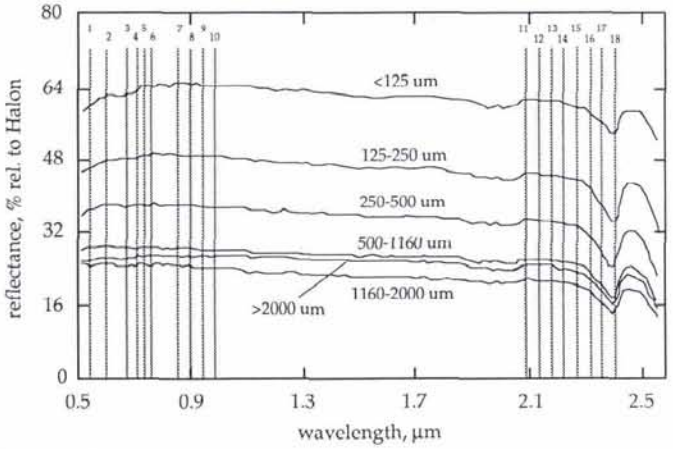

FIG. 12. Effects of particle size on reflectance in limestone. Spectra are not offset.

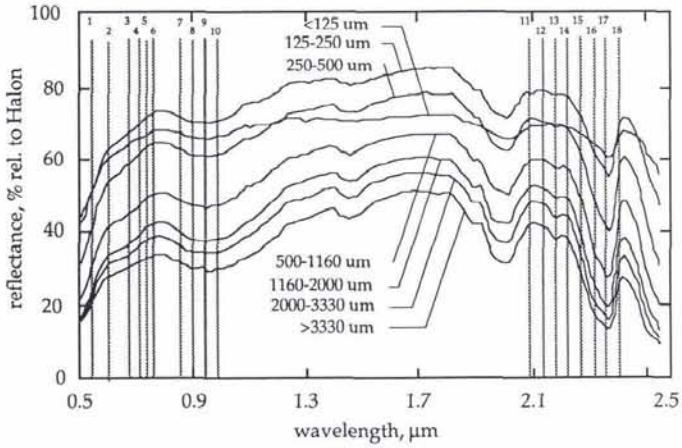

FIG. 13. Effects of particle size on reflectance in dolomite. Spectra are not offset.

material (Crowley, 1986; Rowan *et al.*, 1990). Several factors support the effects of organic matter as an explanation for the spectral variation in the rocks examined for this work.

First, the limestone spectra (and, to a lesser extent, the dolomite) are muted in comparison to other carbonate data. In the range from 2.2 to 2.35 μm, Crowley's data (1986, Figure 1) show the spectral contrast of the carbonate absorption feature ranging from approximately 30 to 45 percent for various limestones. Hunt and Salisbury (1971) show changes in the same wavelength range from 45 to 55 percent for the coarsest size fractions in their two calcite spectra and 25 to 35 percent for their two dolomite samples. The limestones in this study (excluding the bleached limestone) typically showed a 2.2- to 2.35-μm contrast of 10 to 15 percent with a maximum of 25 percent. The highest contrast in any of the dolomite samples in this study was 35 percent, but the majority fell between 20 and 25 percent. These values would suggest that the limestones in this study exhibit significantly lower than standard reflectances, while the dolomites are slightly lower.

This difference and the spectral variations between the limestone and dolomite could be explained by the presence of a hydrothermally mobile, spectrum-quenching impurity in the original limestone. When the dolomitizing fluids altered the limestone, they leached this impurity. The leaching capability of the hydrothermal fluids persisted beyond the dolomitization front to remove the impurity from the limestone while not affecting the calcitic composition. This would explain the presence of the bleached limestone and why it exhibits a purer calcite spectrum.

The dark foliations interpreted as relict or transposed bedding planes also support this hypothesis. These foliations occur in the limestone near the dolomitization front and near any veins of bleached limestone that extend into the limestone. The bleached limestone veins do not occur in locations where the foliations are not present. These foliations would represent the redeposition of the quenching impurity along the paths of fluid flow.

Organic matter, now degraded to near-elemental compounds, makes a convenient choice for this impurity. Crowley (1986) has documented its quenching capabilities and the carbonaceous character of many other units in the district suggests its presence is quite possible. Analysis of minor constituents in the samples will be required to resolve this question. At the time of this writing, however, the instrumentation for quantitative determination of organic content in the samples was unavailable; this work is still in progress.

SUMMARY AND CONCLUSIONS

Spectral imagery at 6-m resolution from the Geoscan MkII airborne multispectral scanner was compared to ground-truth mapping in delineating the distribution of dolomitization in a calcite marble. Contrast stretching of Geoscan band differences showed a good to very good correlation between the imagery and the ground distribution of the hydrothermal alteration associated with the dolomitization event at both 1:2400 and 1:600 mapping scales. Overall, the best results were obtained using channels 7-1 (0.830 to 0.522 μm) and 14-17 (2.176 to 2.308 μm); however, in the IR most difference images taking advantage of the carbonate absorption feature in channel 17 showed an acceptable separation. Factors affecting the results at the more detailed mapping scale included arbitrary cutoffs in defocusing the surface map to "limestone," "dolomite," and "mixed" pixels and disregarding the effects of iron-stained quartz veins that may have been locally abundant enough to have influenced the spectral signature.

Offset corrections based on laboratory spectra of field samples proved useful in transforming image brightness data to a form comparable to laboratory reflectance data. While rudimentary, this correction provides a simple, quick means of calibrating Geoscan imagery.

Examination of textural and particle size effects suggest these were not significant factors in the spectral discrimination of the calcitic and dolomitic marbles. Field relations suggest hydrothermal alteration associated with the dolomitization event flushed a spectrally quenching impurity from the limestone, resulting in the more reflective, higher contrast spectrum of bleached limestone and dolomite. The presence of organic matter in carbonates has been shown to quench reflectance properties (Crowley, 1986); this property and the common occurrence of carbonaceous units in the district suggest organic matter as the likely impurity.

Most remote sensing evaluations of hydrothermally altered lithologies concentrate on the distribution of minerals formed as a result of the alteration. In this study, the airborne imagery could not readily discriminate between the hydrothermal dolomite and the bleached limestone (two compositionally different lithologies) but readily separated the calcite marble from the bleached limestone (two compositionally similar lithologies). The results of this study indicate it is often equally important to consider the spectral effects of what has been removed during alteration as well as what has been added or created.

ACKNOWLEDGMENTS

We would like to thank Frank Honey and Geoscan Pty. Ltd. for providing us with the imagery of the Ludwig skarn. This project would not have been possible without funding from the McGee Fund of Stanford University. Marco Einaudi provided much-appreciated critical commentary on the text and was a steady source of information for geological detail of the district. The first author would also like to thank his field assistants, Dasha Sinitsyna and Elizabeth Zbinden, for their time and effort, as well as Robert and June Thomas for their warm hospitality during his stay in Yerington.

REFERENCES

Crowley, J. K., 1986. Visible and Near-Infrared Spectra of Carbonate Rocks: Reflectance Variations Related to Petrographic Texture and Impurities. *Journ. of Geophysical Res.* 91:5001–5012.

Einaudi, M. T., 1977. Petrogenesis of the Copper-Bearing Skarn at the Mason Valley Mine, Yerington District, Nevada. *Econ. Geol.* 72:769–795.

Einaudi, M. T., L. D. Meinert, and R. J. Newberry, 1981. Skarn Deposits. *Econ. Geol. 75th Anniversary Volume* (B. Skinner, ed.), Econ. Geol. Pub. Co.: El Paso, Texas.

Harris, N. B., 1979. *Skarn Formation near Ludwig, Yerington District, Nevada.* Unpublished Phd thesis, Stanford University, 173 p.

Harris, N. B., and M. T. Einaudi. 1982. Skarn Deposits in the Yerington District, Nevada: Metasomatic Skarn Evolution near Ludwig. *Econ. Geol.* 77:877–898.

Hunt, G. R., and J. W. Salisbury, 1971. Visible and Near-Infrared Spectra of Minerals and Rocks: II. Carbonates. *Modern Geol.* 2:23–30.

Lyon, R. J. P., and F. R. Honey, 1989. Spectral Signature Extraction from Airborne Imagery Using the Geoscan MkII Advanced Airborne Scanner in the Leonora, Western Australia Gold District. *Proceedings IGARSS '89 / 12th Canadian Symposium on Remote Sensing,* Vancouver, B.C., 10-14 July 1989. 5:2925–2930.

———, 1991. Extraction of Thermal Exitance Spectra (TIR) from Geoscan MkII Scanner Imagery: Spectra Derived From Airborne (Mobile) and Ground (Stationary) Imagery Compared with Spectra from Direct Exitance Spectrometry. *Proceedings of the Eighth Thematic Conference on Geologic Remote Sensing,* Denver, Colorado, 29 April - 2 May 1991. 1:117–130.

Knopf, A., 1918. *Geology and Ore Deposits of the Yerington District, Nevada:* U.S.G.S. Prof. Paper 114. 68 p.

Proffett, J. M., 1977. Cenozoic Geology of the Yerington District, Nevada, and Implications for the Nature and Origin of Basin and Range Faulting. *GSA Bull.* 88:247–266.

Roberts, D. A., Y. Yamaguchi, and R. J. P. Lyon, 1986. Comparison of Various Techniques for Calibration of AIS Data. *Proceedings of the 2nd Airborne Imaging Spectrometer Data Analysis Workshop, May 6, 7, 8, 1986.* (G. Vane and A. Goetz, eds.), Jet Propulsion Laboratory, California Institute of Technology: Pasadena, California, pp. 21–30.

Rowan, L. C., O. D. Jones, and M. J. Pawlewicz, 1990. The Use of Visible and Near-Infrared Spectral Reflectance for Estimating the Thermal Maturity of Organic Matter in Sedimentary Rocks. *Fifth Australasian Remote Sensing Conference,* Perth, W. Australia, 8-12 Oct 1990. v. 2.

Rubin, T. D., 1991. Spectral Alteration Mapping with Imaging Spectrometers. *Proceedings of the Eighth Thematic Conference on Geologic Remote Sensing,* Denver, Colorado, 29 April - 2 May 1991. 1:13–25.